*Mon. Not. R. astr. Soc.* (1983) **205**, 605–624

# A complete galaxy redshift sample – I. The peculiar velocities between galaxy pairs and the mean mass density of the Universe

A. J. Bean[1], G. Efstathiou[2], R. S. Ellis[1], B. A. Peterson[3] and T. Shanks[1]

[1]*Department of Physics, University of Durham, South Road, Durham DH1 3LE*
[2]*Institute of Astronomy, Madingley Road, Cambridge CB3 0HA*
[3]*Mount Stromlo and Siding Spring Observatories, Private Bag, Woden, Canberra ACT 2606, Australia*

Received 1983 February 20; in original form 1982 November 25

**Summary.** We have measured redshifts for a new sample of 320 galaxies complete to $J \approx 17$. The two-point correlation function has been estimated using both redshift and positional information. This has been used to estimate the mean-square relative peculiar velocities $\langle w^2 \rangle$ for galaxy pairs with projected separations in the range $0 \leqslant \sigma \leqslant 4\,h^{-1}$ Mpc ($h$ is Hubble's constant in units of $100\,\mathrm{km\,s^{-1}\,Mpc^{-1}}$). We find line-of-sight velocity differences of $\langle w^2 \rangle^{1/2} = 250 \pm 50\,\mathrm{km\,s^{-1}}$ independent of projected separation. The two-point correlation function is well approximated by the power-law model $\xi(r) = (r_0/r)^{1.8}$ with $r_0 = (4.1 \pm 0.3)\,h^{-1}$ Mpc. In addition, we estimate the amplitude of the three-point correlation function. We find $Q = 0.60 \pm 0.06$, where $Q$ is the ratio of the three-point correlation function to the square of the two-point function. These results are used in the cosmic virial theorem to obtain an estimate of the contribution to the mean density from material that is clustered like galaxies. The result is $\Omega = 0.14 \times 2^{\pm 1}$. In order for our results to be compatible with a high density Universe ($\Omega = 1$), most of the dark material must be in a component that is much less strongly clustered than galaxies on scales of $4\,h^{-1}$ Mpc or less.

## 1 Introduction

Our understanding of galaxy clustering has improved greatly in recent years. The statistical studies of Peebles and co-workers (Peebles 1980a and references therein) have provided valuable quantitative data on the clustering pattern and these have proved to be important tests of theories of galaxy formation (see Fall 1979 for a review). However, most of these statistical studies have used the coordinates of galaxies projected on to the sky. If radial velocities were available for a large sample of galaxies they would provide important information about the *dynamics* of galaxy clustering as well as allowing a more detailed study of

the galaxy distribution. For example, two important problems that a redshift catalogue might help to answer are (a) whether the galaxy correlation functions accurately measure the mass distribution and (b) how much dark material is distributed like the galaxies.

Evidence for 'missing' mass comes from applications of the virial theorem to the cores of rich clusters of galaxies and to groups of galaxies (see, e.g. the reviews by Faber & Gallagher 1979; Peebles 1980b), but these methods do not yet give a reliable estimate of the mean density of the dark material. It is difficult to judge whether the material in the cores of rich clusters is representative of that in the rest of the Universe and there are substantial uncertainties in estimates of the masses of groups because of the difficulties involved in assigning group membership. One way of avoiding these problems is to use statistical methods which do not require the assignment of galaxies to particular groups and which may be applied to randomly chosen samples of galaxies. A first step towards such a method was made by Geller & Peebles (1973). More recently, Peebles (1976a, b) has discussed a cosmic virial theorem in which an estimate of the cosmological density parameter $\Omega$ is derived from estimates of the mean-square relative peculiar velocity between galaxy pairs $\langle w^2 \rangle$ and the two- and three-point correlation functions. Here it is assumed that the gradient in 'pressure' due to peculiar velocities is balanced by the gravitational forces from all neighbouring galaxies, which is given by an integral over the three-point function. If the two-point function is modelled as a power law, $\xi(r) = (r_0/r)^{1.8}$ (Peebles 1974) and the three-point function is modelled as $\zeta = Q\xi^2$ (see equation 11 below), the relation predicts $\langle w^2(r) \rangle \propto Q r_0^{1.8} \Omega r^{0.2}$. Thus, the relative peculiar velocities are expected to be almost independent of pair separation. This result requires that the clustering is stable at small separations and that the galaxy correlation functions accurately measure the distribution of mass (see Peebles 1980a, section 72 for a detailed discussion).

Several applications of the cosmic virial theorem may be found in the literature. Davis, Geller & Huchra (1978) found an rms peculiar velocity of $\langle w^2 \rangle^{1/2} \sim 300\,\mathrm{km\,s^{-1}}$ for galaxy pairs of separation $1\,h^{-1}\,\mathrm{Mpc}$★ using a redshift catalogue almost identical to the Shapley–Ames (1932) sample. Applying the cosmic virial theorem they deduced $0.2 < \Omega < 0.7$. Peebles (1979, hereafter P79), using the Kirshner, Oemler & Schechter (1978, hereafter KOS) redshift survey, found $\langle w^2 \rangle^{1/2} \sim 500\,\mathrm{km\,s^{-1}}$ and $\Omega = 0.4 \pm 0.2$. From the redshift catalogue compiled by Rood (1981, unpublished), Peebles (1981) obtained $\langle w^2 \rangle^{1/2} \sim 450\,\mathrm{km\,s^{-1}}$ and $\Omega = 0.60 \pm 0.25$. It is difficult to judge whether the estimates of $\langle w^2 \rangle^{1/2}$ and $\Omega$ deduced from these studies are reasonable. The redshift samples are either small, incomplete or biased to some extent by the Local Supercluster. What is required is a well-controlled survey, with accurate radial velocities, that is large enough to provide a fair sample.

Here, we present an analysis of a new redshift catalogue that we have compiled over the last few years using the Anglo-Australian telescope. The survey consists of 320 galaxies, is complete to $J \sim 17$ in five well-separated fields and, in most cases, radial velocities have been measured to an accuracy of better than $50\,\mathrm{km\,s^{-1}}$. The depth of the sample ensures that the results will not be affected by local inhomogeneities and because the survey is quite large and has not been biased either towards or away from rich clusters it may provide a useful approximation to a fair sample. We describe the survey in more detail in Section 2. The techniques used to estimate the two-point galaxy correlation function and the amplitude of the three-point function are presented in Section 3. In Section 3.4 we test our methods against Monte Carlo simulations designed to match the size and statistical properties of the redshift sample and we discuss the method used to measure the relative peculiar velocities. The main results are presented in Section 4 and are compared with those from the KOS survey and with the recent results of Davis & Peebles (1983). The results are discussed in Section 5.

★ Throughout this paper $h$ is Hubble's constant $H_0$ in units of $100\,\mathrm{km\,s^{-1}\,Mpc^{-1}}$.

## 2 The survey

Details of the survey are given in a separate publication (Peterson *et al.* 1983, Paper III, in preparation) which contains the complete catalogue and a discussion of the photometric and spectroscopic procedures. Here we summarize the basic points.

Five well-separated high-latitude Schmidt fields were chosen as randomly as possible given the availability of photographic material. For each field, an area of 14 square degrees was selected and a list of galaxies to $J > 17.4$ was derived via automated scans of sky-limited Schmidt plates ($J$ = Kodak IIIa-J plus Schott GG395). Galaxies in these lists were subsequently phometered on shorter exposure plates to avoid saturation effects for the brighter galaxies. Calibration was achieved via photoelectric photometry of standard stars and the relative magnitude scale was further checked using secondary images produced by a Pickering (sub-beam) prism.

Using the 3.9-m Anglo-Australian telescope and the RGO spectrograph with a grating offering a reciprocal dispersion of 33 Å mm$^{-1}$ at 3700 Å we then observed a complete sample of galaxies in each field to $J \sim 17$. The exact magnitude limit varies slightly from field to field, but each individual field is very nearly a complete sample. A total of 340 redshifts were measured. The areas surveyed, the galaxy counts and the magnitude limits are summarized in Table 1.

With the Image Photon Counting System, each galaxy spectrum was recorded at a resolution of 1 Å from 3700 to 4700 Å and the redshift determined using cross-correlation techniques (Tonry & Davies 1979). From tests of possible intenal and external errors on the derived radial velocities we conclude that our rms velocity error is better than 50 km s$^{-1}$. The error does not appear to correlate with apparent magnitude, velocity, or galaxy type. A fraction of the data (< 20 per cent) was obtained with slightly poorer resolution and has an rms error of < 100 km s$^{-1}$. A detailed discussion of velocity errors is given in Paper III.

As a check of completeness, we list in Table 1 the results of a $\langle V/V_m \rangle$ test (including curvature and $K$-corrections) applied to each of the five fields (Schmidt 1968). The same test was applied to a set of Monte Carlo simulations (see Section 3.4) from which we conclude that none of our fields is seriously incomplete.

## 3 Estimators and methods

### 3.1 THE TWO-POINT CORRELATION FUNCTION $\xi_v(\sigma,\pi)$

We estimate the mean-square peculiar velocity differences between galaxy pairs using techniques similar to those described in P79. These require estimates of the two-point correlation

**Table 1.** The survey fields.

| Field | (1) RA (h m s) | (2) Dec (° ′) | (3) $h$ (°) | (4) $w$ (°) | (5) $m_{J_{lim}}$ | (6) $N_T$ | (7) $N_G$ | (8) $\langle V/V_m \rangle$ |
|---|---|---|---|---|---|---|---|---|
| N1 | 13 40 44 | 0 00 | 3.75 | 3.72 | 16.86 | 72 | 68 | 0.58 |
| N2 | 10 40 09 | 0 01 | 3.68 | 3.66 | 17.00 | 66 | 65 | 0.43 |
| S1 | 0 56 51 | −28 03 | 3.75 | 3.77 | 17.00 | 80 | 74 | 0.57 |
| S2 | 2 02 03 | −49 44 | 3.71 | 3.76 | 17.00 | 66 | 63 | 0.52 |
| S3 | 3 43 38 | −45 00 | 3.91 | 3.92 | 16.75 | 50 | 50 | 0.50 |

Field centres are given in columns (1) and (2). The height of each field is given in column (3) and the width in column (4). Column (6) gives the number of catalogued galaxies brighter than the magnitude limit $m_{J_{lim}}$ (column 5) and column (7) gives the number with measured redshifts.

function using both redshift and positional information. The redshift separation between two galaxies with velocities $v_1$ and $v_2$ separated on the sky by an angle $\theta_{12}$ is

$$s = (v_1^2 + v_2^2 - 2v_1v_2 \cos\theta_{12})^{1/2}/H_0. \tag{1}$$

For small angles, equation (1) gives $s^2 \approx (\pi^2 + \sigma^2)$ where,

$$\pi = (v_1 - v_2)/H_0 \tag{2a}$$

and

$$\sigma = (v_1 v_2)^{1/2}\theta_{12}/H_0. \tag{2b}$$

Thus $\pi$ measures the approximate separation of pairs along the line-of-sight and $\sigma$ measures the approximate separation perpendicular to the line-of-sight.

The mean number of neighbours around galaxy $i$ expected within the interval ($\sigma \pm \delta\sigma/2$, $\pi \pm \delta\pi/2$) is

$$\langle dN_i(\sigma, \pi)\rangle = n_G\,[1 + \xi_v(\sigma, \pi)]\,p\,(v)\,\delta\pi\,\delta A\,(\sigma). \tag{3}$$

Here, $\xi_v(\sigma, \pi)$ is the two-point correlation function, $p(v)$ is the probability that a galaxy with velocity $v$ is included in the catalogue, $n_G$ is the mean space density of galaxies and $\delta A(\sigma)$ is the area of the $\sigma$ ring within the survey boundary (P79, equation 3). Now, consider a catalogue of random points with density $n_R$ distributed within the survey region according to the selection function $p(v)$. The mean number of random points expected around galaxy $i$ is

$$\langle dR_i(\sigma, \pi)\rangle = n_R\,p\,(v)\,\delta\pi\,\delta A\,(\sigma). \tag{4}$$

Thus, an estimate of $\xi_v(\sigma, \pi)$ is given by

$$1 + \xi_v(\sigma, \pi) = \frac{n_R}{n_G}\frac{\sum_i dN_i}{\sum_i dR_i} = \frac{\langle DD\rangle}{\langle DR\rangle}, \tag{5}$$

where the sums extend over all galaxies in the sample which have velocities within some given interval $v_{min} \leqslant v \leqslant v_{max}$. Because the magnitude limits in our sample vary slightly from field to field we cannot straightforwardly apply the methods used in P79 to calculate $\langle dR_i\rangle$. Thus, to generate a random catalogue with the correct selection function we adopt the following simple method. Consider $l$ fields of solid angle $\omega_k$ ordered by magnitude limit ($m_{lim_1} < m_{lim_2} < \ldots < m_{lim_k} < \ldots < m_{lim_l}$). Let $\Omega_k$ be the total solid angle of all fields with magnitude limit $< m_{lim_k}$ and $dn_k(v, m_1, m_2)$ be the number of galaxies in field $k$ with velocities between $v$, $v + dv$ and apparent magnitudes between $m_1$ and $m_2$. An estimate of the mean number of galaxies, $dN_j(v)$, expected in field $j$ with velocities in the interval ($v$, $v + dv$) is given by

$$dN_j(v) = \omega_j \sum_{k=1}^{l} 1/\Omega_k \sum_{i=k}^{j} \omega_i\, dn_i(v, m_{lim_{i-1}}, m_{lim_i}) \tag{6a}$$

and the total number of random points to be generated within the boundary of field $j$ is

$$N_{Rj} = \frac{n_R}{n_G}\sum_{v_{min}}^{v_{max}} dN_j(v), \tag{6b}$$

We take $n_R/n_G = 400$ which is sufficiently large that fluctuations in the pair-count $\langle DR \rangle$ using different sequences of random numbers are a negligible source of error in the estimates of $\xi_v(\sigma, \pi)$.

In practice, we fit $dN_j(v)$ to a cubic polynomial by least-squares giving a smoothed estimate $\langle dN_j(v) \rangle$. This is done to reduce the effects of small-scale clumping on the redshift distribution. Each point in the random catalogue is then given a velocity from the distribution $\langle dN_j(v) \rangle$. The method assumes that the estimate $\langle dN_j(v) \rangle$ is close to what is expected from a fair sample of the Universe. A check of this point, and an alternative way of estimating $\langle dN_j(v) \rangle$, are presented in Section 4.1.

We have checked our technique by estimating $\xi_v(\sigma, \pi)$ for the KOS survey using the estimator given by equation (5) of P79 and comparing with the results obtained using equations (5) and (6). We find excellent agreement. Additional checks of the estimator have been made using Monte Carlo simulations and are described in Section 3.4.

### 3.2 $\langle w^2 \rangle^{1/2}$ AND THE AMPLITUDE OF THE TWO-POINT CORRELATION FUNCTION

The function $\xi_v(\sigma, \pi)$ will differ from the true spatial correlation function $\xi$ because peculiar velocities (and velocity errors) distort the clustering pattern in the $\pi$ direction. Following P79, this effect is modelled as

$$\xi_v(\sigma, \pi) = \int_{-\infty}^{\infty} \xi\,[\{\sigma^2 + (\pi - w/H_0)^2\}^{1/2}]\, f(w)\, dw \tag{7}$$

where $w$ is drawn from the distribution function $f(w)$. A more complex model, which includes streaming motions, is described in Section 4.3. We define the $n$th moment of $\xi_v$ by

$$\Xi_n(\sigma) = \int_0^{\infty} \pi^n\, \xi_v(\sigma, \pi)\, d\pi. \tag{8}$$

Thus, from equation (7)

$$\Xi_0(\sigma) = \int_0^{\infty} \xi\{(\sigma^2 + \pi^2)^{1/2}\}\, d\pi \tag{9a}$$

and,

$$\Xi_2(\sigma) = \frac{\langle w^2 \rangle}{H_0^2}\, \Xi_0(\sigma) + \int_0^{\infty} \pi^2\, \xi\{(\sigma^2 + \pi^2)^{1/2}\}\, d\pi \tag{9b}$$

where

$$\langle w^2 \rangle = \int_{-\infty}^{\infty} f(w)\, w^2\, dw.$$

Equation (9a) is an Abel integral equation and may easily be inverted to provide a direct estimate of $\xi$ but our data are not of sufficiently high quality to warrant such a procedure. Instead, we adopt the power-law model

$$\xi(r) = (r_0/r)^{\gamma}, \qquad \gamma = 1.8 \tag{10}$$

that has been found to provide an excellent fit to the results from the Zwicky and Lick catalogues (Groth & Peebles 1977). The amplitude of the two-point function may be found using equations (9a) and (10). To estimate $\langle w^2 \rangle$ we may use equations (9b) and (10) as in

P79. Alternatively we can adopt a model for the distribution function $f$ and adjust the parameters to find the best fit to $\xi_v(\sigma, \pi)$. Tests of both methods are discussed in Section 3.4.

### 3.3 THE AMPLITUDE OF THE THREE-POINT CORRELATION FUNCTION

Peebles & Groth (1975) and Groth & Peebles (1977) have shown that the three-point galaxy correlation function $\zeta$ is well approximated by

$$\zeta(r_1, r_2, r_3) = Q\{\xi(r_1)\xi(r_2) + \xi(r_2)\xi(r_3) + \xi(r_3)\xi(r_1)\} \tag{11a}$$

with

$$Q = 1.29 \pm 0.21. \tag{11b}$$

The value of $Q$ deduced from these studies depends weakly on the assumed form of the galaxy luminosity function and on the cosmological model. Clearly our sample is too small to improve on these results but an independent estimate of $Q$ using the redshift sample provides an important check on whether the survey is representative. If $Q$ deduced from the survey is small compared with equation (11b) one might suspect that the sample is biased against rich clusters, whereas if $Q$ is large, the sample may be biased against loose groups.

We have estimated $Q$ using a program which P. J. E. Peebles has kindly made available to us and which was used to estimate $Q$ for the Rood (1981, unpublished) sample (Peebles 1981). We measure the two- and three-point functions projected in the $\pi$ direction,

$$w_v(\sigma) = \frac{\langle DD \rangle}{\langle DR \rangle} - 1, \tag{12a}$$

$$z_v(\sigma, u, v) = \frac{\langle DDD \rangle - \langle DDR \rangle}{\langle DRR \rangle} + 2, \tag{12b}$$

where $\sigma = \sigma_1$, $u = \sigma_2/\sigma_1$, $v = (\sigma_3 - \sigma_2)/\sigma_1$, $\sigma_1 < \sigma_2 < \sigma_3$. The random catalogues used in forming the pair and triplet counts in equation (12) are generated using the method described in Section 3.1. To minimize the effects caused by errors in the background correction we eliminate the contributions to the pair and triplet counts from weakly correlated galaxies by imposing a maximum pair separation $\pi < \pi_c$. If $\sigma_3 \ll \pi_c$ and $\langle w^2 \rangle^{1/2} \ll \pi_c H_0$, $Q$ is given by

$$Q(\sigma, u, v) = z_v(\sigma, u, v) / \{w_v(\sigma) w_v(u\sigma) + w_v(u\sigma) w_v[\sigma(u+v)] + w_v[\sigma(u+v)] w_v(\sigma)\}. \tag{13}$$

### 3.4 TESTS OF THE METHODS USING MONTE CARLO SIMULATIONS

#### *3.4.1 Description and choice of model parameters*

We have tested the methods described above against a series of Monte Carlo simulations based on the hierarchical clustering model. The prescription has been described in detail by Soneira & Peebles (1977, 1978) so we summarize only the main feature of the models. We randomly distribute a fixed number of hierarchical clumps within each field volume. Each clump has a radius $r_1 = 8\,h^{-1}$ Mpc within which we generate two centres at random. At the next level of the hierarchy we draw a smaller sphere of radius $r_2 = r_1 \lambda^{-1}$ around each centre and generate two more centres at random within each sphere. This is repeated so that on the $L$th level of the hierarchy there are $2^L$ points in $2^{L-1}$ spheres of radius $r_1 \lambda^{-(L-1)}$. To get

the observed slope for the two-point correlation function at $r < 8\,h^{-1}$ Mpc we choose $\lambda = 1.78$ and to ensure that the power-law form extends to small scales we take $L = 9$, corresponding to a sphere of radius $79.5\,h^{-1}$ kpc. Each point is then assigned an absolute magnitude within the range $-17.15 > M_J > -22.65$ drawn at random from a Schechter (1976) function with parameters $M_J^* = -19.45$, $\alpha = -1.0$, which approximates the luminosity function deduced from the AAT sample (Efstathiou *et al.* 1983, Paper II, in preparation, section 4.1). The faint end cut-off in the luminosity function is used because it eliminates the large number of faint galaxies that would not be detected in a magnitude limited sample and significantly speeds up the computations. A particle is included in the catalogue if its apparent magnitude (including a K-term of $3z$) is brighter than the required magnitude limit. If we select on average 57 particles per clump for inclusion in the catalogue, we obtain an amplitude for the two-point function of $r_0 = 4.8\,h^{-1}$ Mpc, similar to the value deduced for our survey (Section 4.2). In addition to the uniform Hubble velocity, we assign each particle a peculiar velocity along the line-of-sight $v_p$ which is randomly drawn from the Gaussian distribution $f(v_p) \propto \exp\{-v_p^2/2\langle v_p^2\rangle\}$. Thus the relative peculiar velocities between pairs also follow a Gaussian distribution with $\langle w^2\rangle = 2\langle v_p^2\rangle$.

These simulations are fairly crude approximations to the observed clustering distribution. The two-point correlation function is a good approximation to the power-law model (equation 10) at small separations, but falls off more steeply at $r > 8\,h^{-1}$ Mpc. The three-point function has the correct shape (equation 11a) but with $Q \sim 0.5$ which is significantly lower than that measured from the Zwicky and Lick catalogues (equation 11b), though it is not very different from the value deduced from our redshift survey (Section 4.2). As a further approximation we ignore the small variations in the magnitude limits and solid angles between fields in the real survey. Thus, in each simulated catalogue we generate five fields of area $3.8^\circ \times 3.8^\circ$ with a magnitude limit $J = 17.0$. The mean number of particles per simulated catalogue is $\langle N\rangle = 322$ and we have analysed 40 catalogues with $\langle w^2\rangle^{1/2} = 200\,\mathrm{km\,s^{-1}}$ and 40 with $\langle w^2\rangle^{1/2} = 500\,\mathrm{km\,s^{-1}}$.

### *3.4.2 Tests of the methods*

There are several difficulties associated with using equation (9b) to estimate $\langle w^2\rangle$. The second moment $\Xi_2(\sigma)$ is difficult to measure because small uncertainties in the estimates of $\xi_v$ at large $\pi$ are heavily weighted. Also, the second term on the right-hand side of equation (9b) is divergent if the two-point function is modelled as a power law with $\gamma = 1.8$. These features suggest that we truncate the moments $\Xi_0(\sigma)$ and $\Xi_2(\sigma)$ at some value $\pi_{max}$ (*cf.* P79).

Fig. 1 shows results for $H_0\Xi_2^{1/2}(\sigma)\Xi_0^{-1/2}(\sigma)$ calculated from both sets of simulations with the moments truncated at $\pi_{max} = 10\,h^{-1}$ Mpc. The moments were calculated directly from $\xi_v(\sigma,\pi)$ which was estimated independently for each catalogue using the methods discussed in Section 3.1. The error bars in Fig. 1 show the standard deviation on the mean. The dashed lines show the results of numerically integrating equation (7) using a Gaussian distribution function and the power-law model for $\xi$. These curves predict higher values than the corresponding estimates from the simulated catalogues. This is not due to a systematic error in the analysis technique, rather it is because the model predictions are sensitive to the precise shape of $\xi(r)$ at large separations. The solid curves show predictions when the power-law correlation function is truncated so that $\xi(r) = 0$ at $r > 8\,h^{-1}$ Mpc. This model is a better approximation to the correlation function of the Monte Carlo simulations and the solid curves provide a much better fit to the moment results than do the dashed curves. This comparison shows that our techniques are essentially unbiased. It also illustrates that if the relative peculiar velocities are less than about $500\,\mathrm{km\,s^{-1}}$, estimates of $\langle w^2\rangle^{1/2}$ made using second moments of $\xi_v$ are likely to be highly uncertain because the shape of the correlation

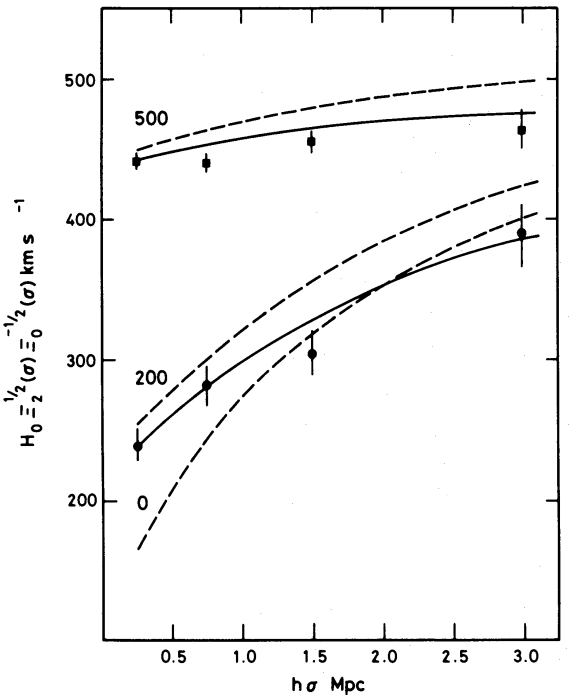


**Figure 1.** Results obtained using moments of $\xi_v(\sigma, \pi)$ from the Monte Carlo simulations. The squares show the mean values from 40 simulations in which the rms relative peculiar velocity was fixed at 500 km s$^{-1}$ and the circles show similar results for $\langle w^2\rangle^{1/2} = 200$ km s$^{-1}$. The error bars give one standard deviation. The dashed lines show the results expected for three values of $\langle w^2\rangle^{1/2}$ (0, 200 and 500 km s$^{-1}$) with the correlation function modelled as a power law, $\xi(r) \propto r^{-1.8}$, and the solid lines show results in which the power law was truncated so that $\xi(r) = 0$ for $r > 8h^{-1}$ Mpc.

function on scales $> 5h^{-1}$ Mpc is poorly determined (Groth & Peebles 1977). This problem cannot be solved by varying $\pi_{max}$ for as $\pi_{max}$ is reduced, the quantity $H_0\Xi_2^{1/2}\Xi_0^{-1/2}$ becomes progressively more insensitive to $\langle w^2\rangle^{1/2}$.

We have adopted a simple curve fitting method which avoids these problems. We minimize the statistic

$$p^2 = \sum_{\pi=0}^{\pi_{max}} \frac{\{\xi_v^0(\sigma,\pi) - \xi_v^p(\sigma,\pi)\}^2}{\delta\xi_v^2(\sigma,\pi)} \tag{14a}$$

where $\xi_v^0(\sigma,\pi)$ is measured from the redshift survey, $\xi_v^p(\sigma,\pi)$ is calculated from equations (7) and (10) with $r_0$ and $\langle w^2\rangle^{1/2}$ as adjustable parameters and

$$\delta\xi_v(\sigma,\pi) = \left\{\frac{(1+\xi_v^p)}{\langle DR\rangle^o}\right\}^{1/2} \simeq \frac{\{\langle DD\rangle^p\}^{1/2}}{\langle DR\rangle^p} \tag{14b}$$

where $\langle DR\rangle^o$ is the measured pair count defined in equation (5). (In equations 14 the superscript o refers to 'observed' quantities and the superscript p refers to 'predicted' quantities). The error estimate in equation (14b) is based on the idea that the errors in $\xi_v$ are dominated by errors in the direct pair count $\langle DD\rangle$ and that $\delta\langle DD\rangle \sim \langle DD\rangle^{1/2}$. The Monte Carlo models give $\delta\langle DD\rangle \simeq 3/2\langle DD\rangle^{1/2}$, thus we expect equation (14a) to approximate a $\chi^2$ statistic.

Table 2 lists the results obtained when this method is applied to the simulated catalogue. The method works extremely well. There is only a slight bias, for large values of $\sigma$, and this

**Table 2.** Model fitting method applied to the Monte Carlo simulations.

| $\sigma$ $h^{-1}$ Mpc | $\langle w^2\rangle^{1/2} = 200$ km s$^{-1}$ $\langle w^2\rangle^{1/2}$ (km s$^{-1}$) | sd | $\langle w^2\rangle^{1/2} = 500$ km s$^{-1}$ $\langle w^2\rangle^{1/2}$ (km s$^{-1}$) | sd |
|---|---|---|---|---|
| 0–0.5 | 210 ± 6 | 40 | 490 ± 13 | 83 |
| 0.5–1.0 | 203 ± 8 | 50 | 463 ± 13 | 79 |
| 1.0–2.0 | 205 ± 13 | 85 | 463 ± 15 | 92 |
| 2.0–4.0 | 189 ± 37 | 233 | 430 ± 34 | 215 |

Here we give the mean value of $\langle w^2\rangle^{1/2}$ determined from 40 simulated catalogues with $\langle w^2\rangle^{1/2} = 200$ km s$^{-1}$ and for 40 catalogue with $\langle w^2\rangle^{1/2} = 500$ km s$^{-1}$ using the model fitting method described in Section 3.4.2. The columns sd give the standard deviation of the estimate from one catalogue.

is probably partly because of inaccuracies in the model for $\xi(r)$. The results are not very sensitive to the choice of $\pi_{max}$, particularly if $\langle w^2\rangle^{1/2} < 500$ km s$^{-1}$. We have repeated the model fits treating $\langle w^2\rangle^{1/2}$ as an adjustable parameter with $r_0$ fixed at $4.8\,h^{-1}$ Mpc. The results are similar to those in Table 2 for $\sigma < 1\,h^{-1}$ Mpc but we find that $\langle w^2\rangle^{1/2}$ is biased towards high values when $\sigma > 2\,h^{-1}$ and $\xi_v(\sigma,\pi) \sim 1$. We therefore allow both $r_0$ and $\langle w^2\rangle^{1/2}$ to vary in the analysis described below.

The main problem in applying this method to the redshift survey lies in the correct choice of the distribution function $f(w)$. One clue comes from the $N$-body simulations of Efstathiou & Eastwood (1981). In these models, the distribution function is quite well approximated by,

$$f(w) = 0.476\,\langle w^2\rangle^{-1/2} \exp\,\{-0.7966\,|w|^{3/2}\langle w^2\rangle^{-3/4}\} \tag{15a}$$

and the shape is fairly weakly dependent on pair separation. Peebles (1976b, 1979) has argued that a good fit to the observations may be obtained using an exponential,

$$f(w) = 2^{-1/2}\langle w^2\rangle^{-1/2} \exp\,\{-2^{1/2}\,|w|\,\langle w^2\rangle^{-1/2}\}. \tag{15b}$$

In Section 4.3 we examine the sensitivity of the results on the assumed form of $f(w)$ and we describe possible effects due to streaming motions.

We have also used the Monte Carlo simulations to check the estimator of $Q$ (equations 12, 13 with $\pi_c = 5\,h^{-1}$ Mpc). From 10 models with $\langle w^2\rangle^{1/2} = 500$ km s$^{-1}$ we find $Q = 0.44 \pm 0.03$. These results are in reasonable agreement with the expected value $Q \sim 0.5$.

## 4 Results

### 4.1 ESTIMATION OF $\xi_v(\sigma,\pi)$

Fig. 2 shows the redshift distribution $dN(v)$ (equation 6a) for each of the three magnitude limits used in our survey (Table 1). The polynomial fits used to model the selection function are shown as the solid lines in the figure. An alternative estimate of the selection function can be obtained from the galaxy luminosity function $\phi(M)\,dM$. The expected redshift distribution is

$$\langle dN_j(v)\rangle = \frac{\Omega_j}{H_0^3}\,v^2\left[\int_{-\infty}^{M_c(v)} \phi\,(M)\,dM\right]dv, \tag{16}$$

where,

$$M_c = m_{\mathrm{lim}_j} - 25 - 5\log\,(v/H_0) - kv/c,$$

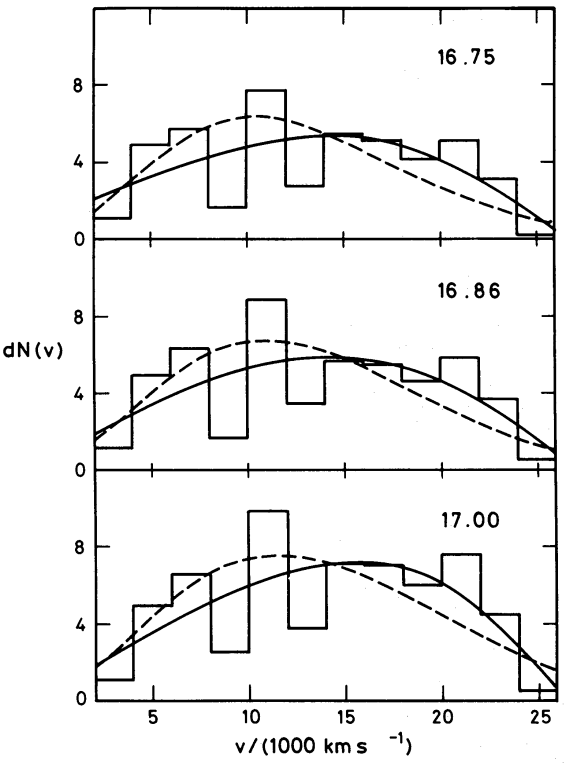


**Figure 2.** The number–redshift relation calculated from equation (6a) and normalized to an area of $3.8° \times 3.8°$ for each of the magnitude limits used in the AAT survey. The solid lines show a least-square fit to a cubic and the dashed lines show the distribution expected from the galaxy luminosity function (equations 16 and 17).

and $k$ represents the K-correction ($3.15z$). In Paper II we estimate $\phi(M)$ using techniques that are unaffected by galaxy clustering. The best fit to a Schechter (1976) function has parameters,

$$M_J^* = -19.44 + 5 \log h, \tag{17a}$$

$$\alpha = -1.00. \tag{17b}$$

A detailed discussion of the errors in these parameters is given in Paper II. In the present application, the normalization constant is fixed by requiring that the total number of galaxies counted within the redshift range shown in Fig. 2 ($2000\ \mathrm{km\,s^{-1}} \leqslant v \leqslant 26\,000\ \mathrm{km\,s^{-1}}$) be equal to the integral of equation (16). The redshift distributions predicted from equation (16) are shown as the dashed lines in Fig. 2. The predicted distributions are quite close to what is observed, though the observations show an overabundance of galaxies with velocities of about $20\,000\ \mathrm{km\,s^{-1}}$ and a deficiency of galaxies with velocities of about $10\,000\ \mathrm{km\,s^{-1}}$. This agrees with the $\langle V/V_m \rangle$ estimates given in Table 1 which are generally slightly larger than 0.5. We take the differences between the dashed and solid lines in Fig. 2 to give a reasonable indication of the uncertainties in our estimates of $\xi_v(\sigma, \pi)$ caused by inaccuracies in modelling the redshift distribution.

In Fig. 3(a) we present estimates of $\xi_v$ for the AAT survey obtained from equations (5) and (6) using the solid lines in Fig. 2. Fig. 3(b) is the equivalent diagram obtained using the dashed lines in Fig. 2 and shows that the estimates of $\xi_v$ are remarkably insensitive to the adopted shape of $\langle dN_j(v) \rangle$. Throughout the rest of this section we use estimates of $\xi_v$ obtained using the polynomial fits to the redshift distribution but we stress that none of our

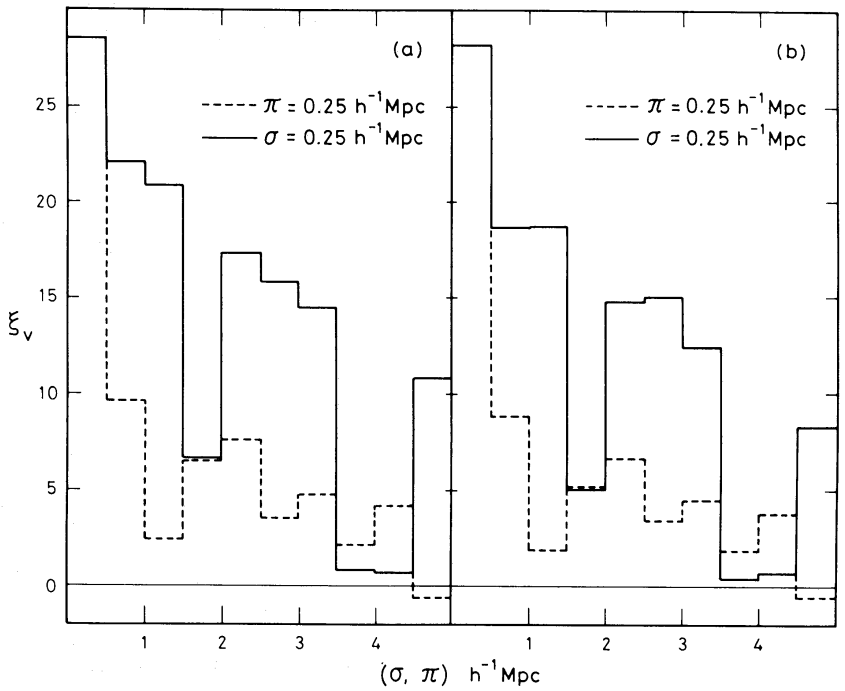


**Figure 3.** $\xi_v(\sigma, \pi)$ for the AAT survey estimated using equation (5). In (a) the selection function is based on the solid lines shown in Fig. 2 and in (b) the selection function is given by the dashed lines in Fig. 2. In each case, the solid histogram shows $\xi_v(\sigma, \pi)$ with $\sigma$ fixed within the range $0 < \sigma < 0.5\,h^{-1}$ Mpc and $\pi$ varying between $0 < \pi < 5\,h^{-1}$ Mpc and the dashed histogram shows $\xi_v$ with $\pi$ fixed and $\sigma$ varying.

numerical results would be altered significantly had we chosen to use the redshift distribution determined from the luminosity function.

### 4.2 THE AMPLITUDES OF THE TWO- AND THREE-POINT CORRELATION FUNCTIONS

Using the power-law model for $\xi(r)$ in equation (9a) we expect,

$$\Xi_0(\sigma) = \frac{r_0^\gamma}{\sigma^{\gamma-1}} \frac{\tau^{1/2}}{2} \frac{\Gamma[(\gamma-1)/2]}{\Gamma(\gamma/2)}. \tag{18}$$

In Fig. 4 we show $\Xi_0(\sigma)$ truncated at $\pi_{max} = 20\,h^{-1}$ Mpc (open circles). To give an indication of possible systematic errors caused by an incorrect estimate of the pair count $\langle DR \rangle$ used in equation (5) we also plot $\Xi_0^c(\sigma) = \Xi_0(\sigma) - \bar{\xi}(\sigma)\pi_{max}$ where $\bar{\xi}(\sigma)$ is the mean value of $\xi_v(\sigma, \pi)$ between $25\,h^{-1}$ Mpc $< \pi < 50\,h^{-1}$ Mpc. These points are plotted as filled circles in Fig. 4. There are no indications of any serious systematic errors except possibly at $\sigma \gtrsim 10\,h^{-1}$ Mpc where $\Xi_0(\sigma) \lesssim 1$. Fitting the first nine points in Fig. 4 to a power law by least-squares and constraining the slope to be $-0.8$ we find,

$$\log \Xi_0(\sigma) = (1.32 \pm 0.04) - 0.8 \log \sigma, \tag{19a}$$

$$\log \Xi_0^c(\sigma) = (1.34 \pm 0.05) - 0.8 \log \sigma. \tag{19b}$$

Note that if the slope is allowed to vary, the least-squares fit to $\Xi_0(\sigma)$ has a slope of $-0.89$ and the fit to $\Xi_0^c(\sigma)$ gives a slope of $-0.75$. Equation (19b) is shown in Fig. 4 and provides quite a good fit to the data, though there is perhaps a hint of a flatter slope at $\sigma \sim 2\,h^{-1}$ Mpc.

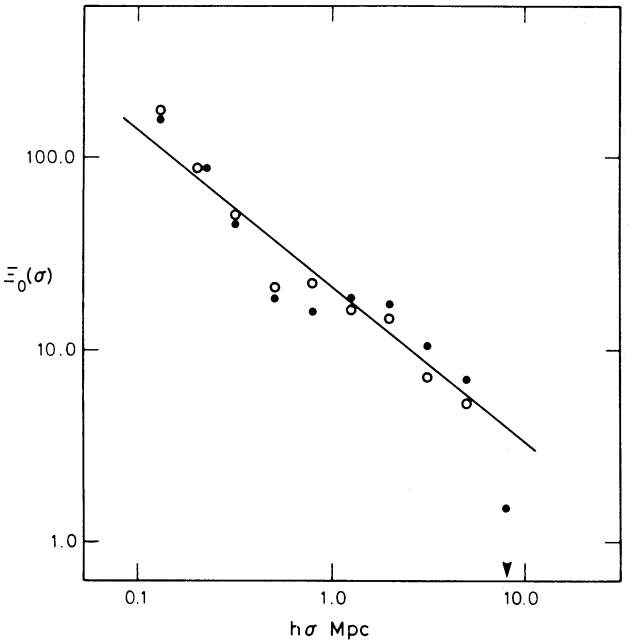


**Figure 4.** Estimates of the zeroth moment of $\xi_V(\sigma, \pi)$ (equation 9a). The open circles show $\Xi_0(\sigma)$ truncated at $\pi_{max} = 20\,h^{-1}$ Mpc and the solid circles give an indication of the effects caused by inaccuracies in the normalization of the background pair count $\langle DR \rangle$ used in equation (5) (see text). The solid line shows the model $\xi(r) = (r_0/r)^{1.8}$ with $r_0 = 4.1\,h^{-1}$ Mpc.

The shape of the two-point function on large scales is discussed in detail by Shanks (1982) and Shanks *et al.* (1983). We find $\xi \approx 0$ on scales between $15\,h^{-1} \lesssim r \lesssim 100\,h^{-1}$ Mpc, which conflicts with the results of Kirshner, Oemler & Schechter (1979) who found $\xi \sim 1$ on scales as large as $r \sim 30\,h^{-1}$ Mpc. This discrepancy is discussed further by Shanks *et al.* (1983).

From equations (18) and (19) we obtain,

$$r_0 = (4.1 \pm 0.3)\,h^{-1}\,\text{Mpc}, \tag{20}$$

which is in excellent agreement with the value $r_0 = 4.2 \pm 0.3\,h^{-1}$ Mpc deduced by Peebles (P79) from the KOS sample. However, Davis & Peebles (1983) find $r_0 = (5.4 \pm 0.3)\,h^{-1}$ Mpc using the Harvard redshift survey (Huchra *et al.* 1983). The discrepancy is probably due to

**Table 3.** $Q$ determined from the AAT survey.

| $\sigma(h^{-1}$ Mpc) | $u$ | | | |
|---|---|---|---|---|
| | 1–2 | 2–3 | 3–4 | |
| 0.125 | 0.64 | 0.92 | 1.39 | $0 < v < 0.5$ |
| | 0.37 | 0.20 | −0.05 | $0.5 < v < 1.0$ |
| 0.375 | 0.09 | 0.57 | 0.68 | $0 < v < 0.5$ |
| | 0.61 | 0.48 | 0.46 | $0.5 < v < 1.0$ |
| 0.750 | 0.25 | 0.62 | 0.71 | $0 < v < 0.5$ |
| | 0.49 | 0.86 | 0.87 | $0.5 < v < 1.0$ |
| 1.500 | 0.49 | 0.51 | 0.94 | $0 < v < 0.5$ |
| | 0.83 | 0.79 | 0.79 | $0.5 < v < 1.0$ |

sampling fluctuations and we emphasize that such an effect is not included in the error estimate given in equation (20).

Table 3 gives results for the parameter $Q$ estimated using equation (13) with $\pi_c = 5\,h^{-1}$ Mpc. The mean value is

$$Q = 0.60 \pm 0.06, \tag{21}$$

where the quoted error is the standard deviation on the mean of the 24 values listed in Table 3. This value is consistent with $Q = 0.68 \pm 0.05$ deduced by Peebles (1981) from the Rood (1981, unpublished) catalogue but is lower than the value obtained by Groth & Peebles (1977) from the Zwicky and Lick catalogues. The discrepancy is not particularly surprising because $Q$ is sensitive to the presence of high density clumps such as the cores of rich clusters. For example, Groth & Peebles (1977) found that when the core of the Coma cluster was excluded from the 15 mag Zwicky catalogue $Q$ decreased from 1.34 to 0.85. The low value of $Q$ in equation (21) indicates that our survey has undersampled such high density clumps. As in the case of the amplitude of the two-point function, this sort of error is not reflected in the error estimate quoted in equation (21).

We have also estimated $Q$ for the KOS survey using the same techniques. We include all galaxies brighter than $J_{KOS} = 15$ with velocities between 2000 and 16 000 km s$^{-1}$. The estimates of $Q$ are noisier in this case because of the smaller size of the sample ($\sim 150$ galaxies) but we find $Q = 1.3 \pm 0.3$ which is consistent with equation (11b). Thus, whilst KOS state that they excluded the Coma cluster from their survey, the amplitude of the three-point function does not indicate any serious bias against high density regions.

### 4.3 THE RELATIVE PECULIAR VELOCITIES

The differences between the solid and dashed histrograms in Fig. 3 clearly show the elongation of the clustering pattern caused by peculiar velocities. In this section we estimate the magnitude of $\langle w^2 \rangle^{1/2}$ using the model fitting method described in Section 3.4.2. We first consider models in which streaming motions are neglected. Fig. 5 shows estimates of $\xi_v(\sigma, \pi)$ together with the best fitting models (equations 7 and 10) taking $\pi_{max} = 10\,h^{-1}$ Mpc and the distribution function of equation (15a). The dashed lines in Fig. 5 show the best fits with $\langle w^2 \rangle^{1/2}$ constrained to be 500 km s$^{-1}$. It is clear that such a high value is a poor fit to the data. We have also fitted models using Gaussian and exponential (equation 15b) distribution functions. The results summarized in Table 4(a) are not particularly sensitive to the choice of $f(w)$.

These estimates of $\langle w^2 \rangle^{1/2}$ are sufficiently small that one might question whether it is reasonable to ignore streaming motions. Using the equation of conservation of particle pairs (Peebles 1976, equation 16) and the power-law model for $\xi$ (equation 10) we would expect the mean relative peculiar velocity between galaxy pairs of separation $r$ to be

$$\langle \mathbf{w} \rangle \simeq -H_0 \bar{\xi} (1 + \xi)^{-1} \mathbf{r} \tag{22}$$

if $\Omega = 1$. Thus $\langle \mathbf{w} \rangle \approx -H_0 \mathbf{r}$ at small separations, as expected if high density clumps are bound and stable with fixed sizes in proper coordinates. Equation (22) predicts $\langle w \rangle \sim -200$ km s$^{-1}$ at $r \sim 4\,h^{-1}$ Mpc, which is comparable to the estimates of $\langle w^2 \rangle^{1/2}$ given in Table 4(a). In a low-density universe, the mean relative peculiar velocities can be substantially smaller than is indicated by equation (22). This effect can be seen in the $N$-body simulations of Efstathiou & Eastwood (1981) and occurs because of the slow growth rate of linear perturbations in a low density model (Peebles & Groth 1976). Rather than attempt to derive a more

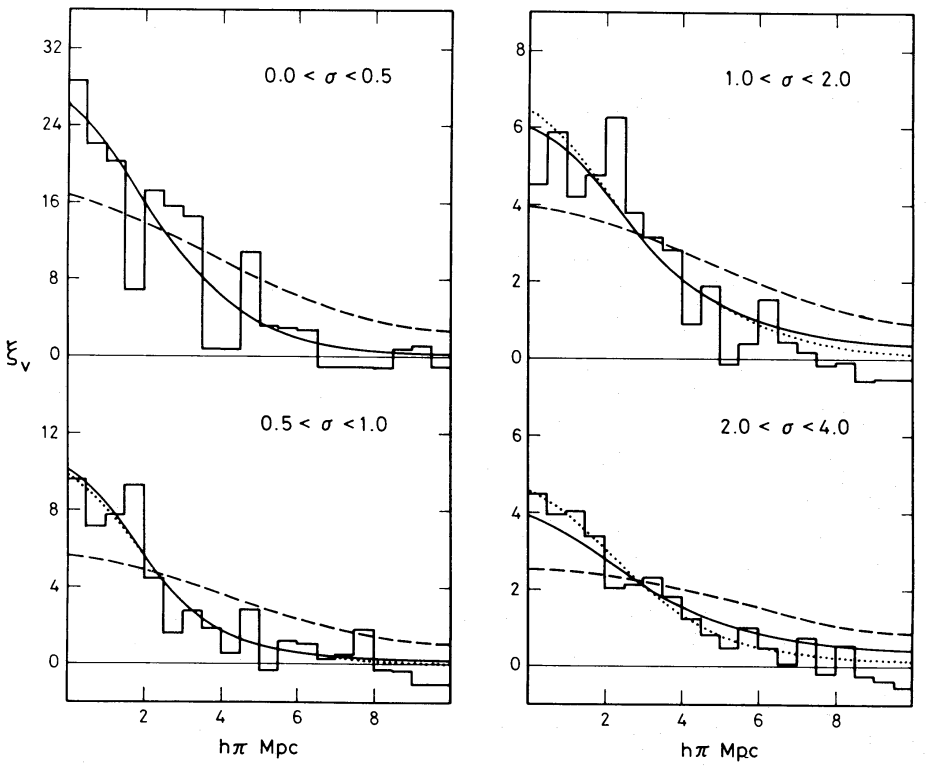


**Figure 5.** Estimates of $\xi_V(\sigma, \pi)$ for the AAT survey. The solid lines show the best fits obtained using the $|w|^{3/2}$ distribution function (equation 15a) neglecting streaming motions. The dotted lines show the best fits for a model which includes streaming motions (equations 22 and 23). The model parameters derived from these fits are given in Table 4(a, b). The dashed lines show the best fits (neglecting streaming) with $\langle w^2 \rangle^{1/2}$ constrained to be 500 km s$^{-1}$. $\sigma$ is given in units of $h^{-1}$ Mpc.

**Table 4.** (a) Model fits to $\xi_V(\sigma, \pi)$ for the AAT survey (no streaming motions).

| $\sigma$ | $G$ | | $\|w\|^{3/2}$ | | $E$ | |
|---|---|---|---|---|---|---|
| | $\langle w^2 \rangle^{1/2}$ | $r_0$ | $\langle w^2 \rangle^{1/2}$ | $r_0$ | $\langle w^2 \rangle^{1/2}$ | $r_0$ |
| 0–0.5 | 230 | 4.4 | 240 | 4.4 | 270 | 4.4 |
| 0.5–1.0 | 150 | 4.1 | 160 | 4.1 | 180 | 4.1 |
| 1.0–2.0 | 180 | 5.1 | 180 | 5.1 | 190 | 5.1 |
| 2.0–4.0 | 0 | 6.2 | 0 | 6.2 | 0 | 6.2 |

(b) Model fits to $\xi_V(\sigma, \pi)$ for the AAT survey (including streaming motions).

| $\sigma$ | $G$ | | $\|w\|^{3/2}$ | | $E$ | |
|---|---|---|---|---|---|---|
| | $\langle w^2 \rangle^{1/2}$ | $r_0$ | $\langle w^2 \rangle^{1/2}$ | $r_0$ | $\langle w^2 \rangle^{1/2}$ | $r_0$ |
| 0–0.5 | 250 | 4.3 | 260 | 4.3 | 300 | 4.4 |
| 0.5–1.0 | 200 | 3.8 | 220 | 3.8 | 260 | 3.9 |
| 1.0–2.0 | 250 | 4.7 | 270 | 4.8 | 320 | 4.9 |
| 2.0–4.0 | 190 | 5.6 | 200 | 5.6 | 220 | 5.6 |

Here we give the values of $\langle w^2 \rangle^{1/2}$ and $r_0$ which provide the best fits to the histograms of $\xi_V(\sigma, \pi)$ shown in Fig. 5. The results are given for three distribution functions: a Gaussian ($G$), the $|w|^{3/2}$ function (equation 15a) and an exponential ($E$). (a) gives results for a model which neglects streaming motions (equation 7) and (b) gives results for a model with streaming motions (equations 22 and 23). $\langle w^2 \rangle^{1/2}$ is given in km s$^{-1}$ and $\sigma$ and $r_0$ are given in units of $h^{-1}$ Mpc.

complicated (and uncertain) model that is applicable for arbitrary $\Omega$ we shall consider equation (22). Since as will be shown in Section 4.4, our results imple a low-density universe we would expect the model to overestimate the effects of streaming motions. The model for $\xi_v(\sigma, \pi)$ is then

$$1 + \xi_v(\sigma, \pi) = \int_{-\infty}^{\infty} [1 + \xi(r)]\, f\, [w_3 + H_0 \xi\, (1 + \xi)^{-1} r_3]\, dw_3, \tag{23}$$

where $r^2 = \sigma^2 + r_3^2$, $r_3 = (\pi - w_3/H_0)$ (*cf.* Peebles 1980a, equation 76; Davis & Peebles 1983, equation 22). In order to simplify the model fitting procedure we fix $r_0 = 4.1\, h^{-1}$ Mpc in the model for the streaming velocities (equation 22). The best fits to $\xi_v(\sigma, \pi)$ using equation (23) are given in Table 4(b) and the results obtained using the $|w|^{3/2}$ distribution function are shown as the dotted lines in Fig. 5. The best-fitting models with $\langle w^2 \rangle^{1/2} = 500\,\mathrm{km\,s^{-1}}$ are not altered very much if streaming motions are included, hence we do not show them in Fig. 5. The inclusion of streaming motions substantially increases the estimates of $\langle w^2 \rangle^{1/2}$ at $\sigma > 1\, h^{-1}$ Mpc and the results become somewhat more sensitive to the shape of the distribution function $f(w)$. Although Peebles (1976a, b) has argued that the exponential distribution provides a good fit to the observations, for the AAT data we find that the Gaussian and the $|w|^{3/2}$ models give smaller values for the statistic $p^2$ and provide the better fits as judged by eye. We, therefore, adopt a value

$$\langle w^2 \rangle^{1/2} = 250 \pm 50\,\mathrm{km\,s^{-1}}, \qquad 0.25\ \mathrm{Mpc} \lesssim h\sigma \lesssim 2\ \mathrm{Mpc} \tag{24}$$

after correction for an rms velocity error of $50\,\mathrm{km\,s^{-1}}$ (Section 2). The error estimate in equation (24) is based on the results from the Monte Carlo simulations and from the spread in the various estimates given in Table 4. This estimate of $\langle w^2 \rangle^{1/2}$ is much greater than the

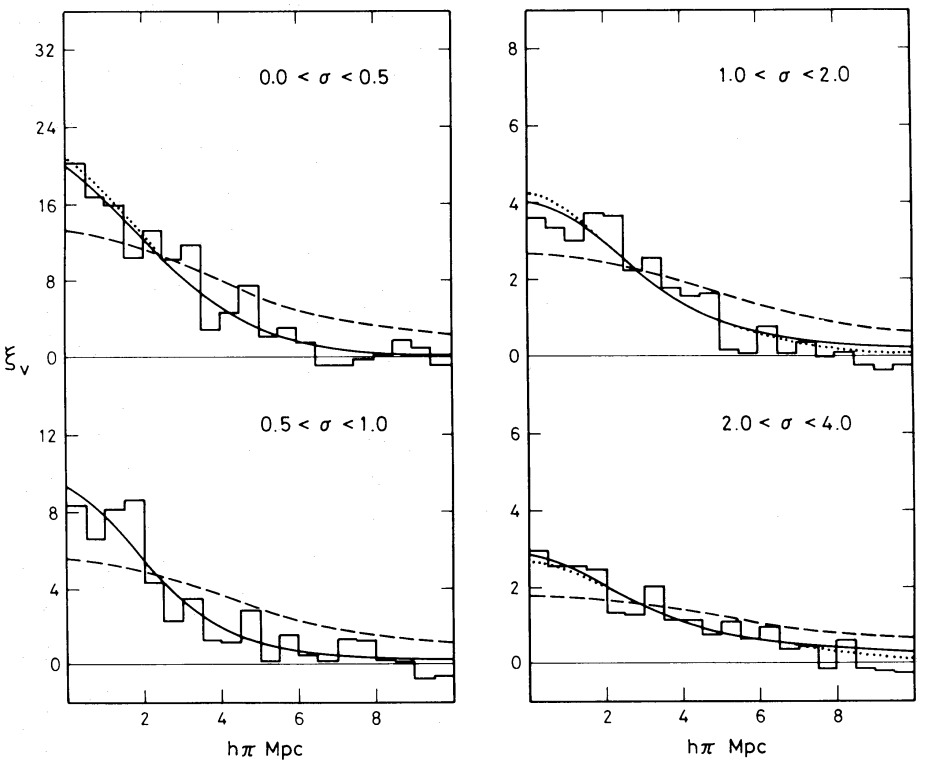


**Figure 6.** As for Fig. 5 except here $\xi_v$ has been determined from the AAT survey combined with the KOS survey. The model parameters derived from the fits are given in Tables 5(a, b).

**Table 5.** (a) Model fits to $\xi_v(\sigma, \pi)$ for the AAT + KOS surveys (no streaming motions).

| $\sigma$ | $G$ | | $\lvert w \rvert^{3/2}$ | | $E$ | |
|---|---|---|---|---|---|---|
| | $\langle w^2 \rangle^{1/2}$ | $r_0$ | $\langle w^2 \rangle^{1/2}$ | $r_0$ | $\langle w^2 \rangle^{1/2}$ | $r_0$ |
| 0–0.5 | 250 | 3.9 | 260 | 3.9 | 310 | 4.0 |
| 0.5–1.0 | 170 | 4.0 | 180 | 4.1 | 210 | 4.1 |
| 1.0–2.0 | 190 | 4.2 | 190 | 4.2 | 210 | 4.2 |
| 2.0–4.0 | 0 | 5.2 | 0 | 5.2 | 0 | 5.2 |

(b) Model fits to $\xi_v(\sigma, \pi)$ for the AAT + KOS surveys (including streaming motions).

| $\sigma$ | $G$ | | $\lvert w \rvert^{3/2}$ | | $E$ | |
|---|---|---|---|---|---|---|
| | $\langle w^2 \rangle^{1/2}$ | $r_0$ | $\langle w^2 \rangle^{1/2}$ | $r_0$ | $\langle w^2 \rangle^{1/2}$ | $r_0$ |
| 0–0.5 | 270 | 3.8 | 280 | 3.9 | 340 | 3.9 |
| 0.5–1.0 | 230 | 3.8 | 240 | 3.9 | 290 | 3.9 |
| 1.0–2.0 | 270 | 3.8 | 280 | 3.8 | 350 | 3.9 |
| 2.0–4.0 | 270 | 4.6 | 290 | 4.7 | 330 | 4.7 |

As for Table 4 except that here fits are to estimates of $\xi_v(\sigma, \pi)$ from the AAT sample combined with the KOS sample which are shown in Fig. 6.

rms velocity errors in the redshift sample hence there is little doubt that we are measuring real peculiar velocities.

It is straightforward to combine our sample with the KOS redshift survey (Efstathiou 1983). The estimates of $\xi_v(\sigma, \pi)$ are shown in Fig. 6 and the parameters determined from the model fits are given in Table 5. The estimates of $\langle w^2 \rangle^{1/2}$ are slightly larger than those in Table 4. At least part of the increase is caused by the larger measurement errors in the KOS survey. For the combined sample we would estimate the rms velocity error to be about $70\,\mathrm{km\,s^{-1}}$. Thus the mean value of $\langle w^2 \rangle^{1/2}$ for the combined samples does not differ greatly from the estimate given in equation (24) suggesting that we have a fairly stable estimate of the relative peculiar velocities.

The estimates of $\langle w^2 \rangle^{1/2}$ presented here are considerably smaller than those derived in most previous studies (see Section 1). They are consistent with the results obtained by Davis & Peebles (1983) using the Harvard redshift sample. They obtain $\langle w^2 \rangle^{1/2} \approx 340 \pm 40\,\mathrm{km\,s^{-1}}$ at projected separations $\sigma \approx 1\,h^{-1}$ Mpc using the exponential distribution function and a model for the streaming motions similar to equation (22). Their values are close to those given in Tables 4(b) and 5(b) for the exponential distribution which shows remarkable consistency in the results from two very different surveys. A significant source of systematic error in the estimates of $\langle w^2 \rangle^{1/2}$ appears to be due to inadequacies in the models for the distribution function $f$. As mentioned above, the exponential distribution function provides a poorer fit to the histograms of $\xi_v$ shown in Figs 5 and 6 than either of the other two distribution functions that we have considered. Also, we have argued that the model describing streaming motions (equation 22) probably overestimates the importance of the effect on scales $\sim r_0$. For these reasons, we consider the result given in equation (24) above to be a reasonable estimate.

### 4.4 APPLICATION OF THE COSMIC VIRIAL THEOREM

Detailed derivations of the cosmic virial theorem have been given by Peebles (1976b, 1980a Section 72). If we consider scales $r$ where $\xi(r) \gg 1$ and the time-scale for evolution of clusters

of size $r$ is smaller than the Hubble time, the relation reads,

$$\frac{\partial}{\partial r}(\xi\langle w_r^2\rangle)+\frac{\xi}{r}\langle 2w_r^2-w_t^2\rangle \simeq -\frac{2G\rho}{r}\int d^3z\,\frac{\mathbf{r}\cdot\mathbf{z}}{(z+\epsilon)^3}\,\xi(r,z,|\mathbf{r}-\mathbf{z}|) \tag{25}$$

(Peebles 1976b, equation 23). Here $\langle w_r^2\rangle$ and $\langle w_t^2\rangle$ are the mean-square relative peculiar velocities in the radial and tangential direction respectively of galaxy pairs with separation $r$; $\rho$ is the mean mass density. The parameter $\epsilon$ is included in equation (25) to illustrate the effects of a cut-off in the gravitational potential due to the finite size of a galaxy. The three-point correlation function is assumed to have the form given in equation (11). If we assume isotropy ($2\langle w_r^2\rangle=\langle w_t^2\rangle$) and $\epsilon=0$, equation (25) gives $\langle w^2(\sigma)\rangle \propto \sigma^{2-\gamma}$ (Peebles 1976a, b). Since the galaxy two-point correlation function gives $\gamma=1.8$ we would expect $\langle w^2(\sigma)\rangle^{1/2} \propto \sigma^{0.1}$ if the galaxy correlation functions measure the distribution of mass on small scales. This is certainly consistent with the weak dependence of $\langle w^2\rangle^{1/2}$ on $\sigma$ found in the previous section.

Fig. 7 shows several models for the line-of-sight velocity dispersion derived from equation (25) using $r_0=4.1\,h^{-1}$ Mpc, $\gamma=1.8$ and a cut-off parameter in the range $0<\epsilon<100\,h^{-1}$ kpc. At separations $\sigma\sim 1\,h^{-1}$ Mpc the results are not very sensitive to the precise value of $\epsilon$. Anisotropy in the velocity dispersions, in the sense of predominantly radial orbits, would tend to act in the opposite direction to increasing $\epsilon$. The numerical simulations of Efstathiou & Eastwood (1981) and the calculations of Davis & Peebles (1977) indicate a substantial anisotropy at separations comparable to $r_0$. These results may be roughly parameterized by the model

$$\frac{\langle w_t^2\rangle}{\langle w_r^2\rangle}=2-\frac{\alpha(r/r_0)}{[1+(r/r_0)^2]},\qquad 1.5\lesssim\alpha\lesssim 2. \tag{26}$$

In Fig. 7 we show a model using equation (26) with $\alpha=2$.

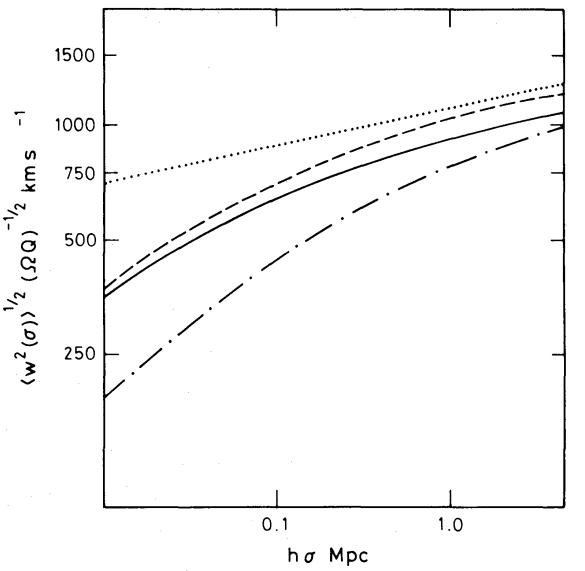


**Figure 7.** Models for the line-of-sight rms relative peculiar velocity using equation (25). The three-point correlation function is modelled according to equation (11) and the two-point function is modelled as a power law, $\xi(r)=(r_0/r)^{1.8}$ with $r_0=4.1\,h^{-1}$ Mpc. The dotted line shows a model in which the cut-off parameter $\epsilon=0$, the solid line shows $\epsilon=10\,h^{-1}$ kpc and the dot–dashed line shows $\epsilon=100\,h^{-1}$ kpc. The dashed line shows a model for anisotropy (equation 26 with $\alpha=2$) and $\epsilon=10\,h^{-1}$ kpc.

As a reasonable compromise between the uncertainties in the theoretical models, we adopt the model shown as the solid line in Fig. 7. Together with equation (24) this gives $Q\,\Omega = 0.09 \pm 0.03$. Adopting $Q = 0.6$ measured from our survey (equation 21) we find $\Omega = 0.14$. It is difficult to estimate the uncertainty in the value of $\Omega$ due to sampling fluctuations. Our value of $Q$ is about a factor of 2 smaller than the value deduced from larger samples ($Q = 1.3$, equation 11b) which suggests that our estimate of $\Omega$ is uncertain by less than a factor of 2. (Since $\langle w^2 \rangle^{1/2}$ and $Q$ are determined consistently for the same galaxy sample we would expect sampling errors to partially cancel in our estimate of $\Omega$.) Thus we conclude,

$$\Omega = 0.14 \times 2^{\pm 1}. \tag{27}$$

An alternative estimate of $\Omega$ may be obtained from the Layzer–Irvine energy equation (Fall 1975). This gives,

$$\langle v_1^2 \rangle \simeq \frac{1}{2} G\rho \int_0^\infty \frac{\xi}{r} d^3\mathbf{r}. \tag{28}$$

There are two major problems in applying this equation. The integral is sensitive to the shape of the two-point function at large scales and is therefore highly uncertain. Also, a model is required to relate the one-dimensional mean-square relative peculiar velocities $\langle w^2 \rangle$ measured for galaxy pairs with separations $\sim 1\,h^{-1}$ Mpc and the mean-square peculiar velocity $\langle v_1^2 \rangle$ that appears in equation (28); $\langle v_1^2 \rangle^{1/2}$ could differ substantially from the estimate given in equation (24) due to large-scale correlated motions (Peebles 1976a). If we assume that $\xi = 0$ on scales larger than $\sim 2r_0$, equation (28) gives

$$\langle v_1^2 \rangle^{1/2} \simeq [3/(2-\gamma)]^{1/2} 2^{-\gamma/2} H_0 r_0 \simeq 850\ \Omega^{1/2}\,\mathrm{km\,s^{-1}},$$

where we have used $r_0 = 4.1\,h^{-1}$ Mpc. Taking $\langle v_1^2 \rangle^{1/2} = (3/2)^{1/2}\,250\,\mathrm{km\,s^{-1}}$ we find $\Omega = 0.13$ in agreement with equation (27). This should not be considered as evidence in favour of the assumption that $\xi$ is exactly zero on large scales because it is possible that our neglect of large-scale correlations (or anti-correlations) together with our simple model for $\langle v_1^2 \rangle$ have combined to produce fortuitous agreement with the cosmic virial theorem. A test of the model can be made by searching for correlated motions on large scales (e.g. Rubin *et al.* 1976; Clutton-Brock & Peebles 1981).

## 5 Discussion and conclusions

The estimate of the cosmic density parameter given in equation (27) is based upon a number of simplifying assumptions and approximations and it is worthwhile to summarize these here.

(1) In estimating the relative peculiar velocities we have adopted several models for the velocity distribution function $f$ and we have considered possible effects due to streaming motions. The models provide good fits to the data as is shown in Figs 5 and 6. However, it is possible that the correct distribution function has a longer tail than any of the functions that we have tried, in which case we could have substantially underestimated $\langle w^2 \rangle$. Results from numerical simulations would argue against this possibility though a direct observational test would require a much larger redshift sample than is presently available.

(2) We have assumed that our survey is large enough that it represents a fair sample of the Universe. There is some evidence which indicates that this assumption may not be justified. The value of $Q$ deduced from our survey is lower than is obtained from larger catalogues suggesting that we have undersampled high density regions. The amplitude of the two-point correlation function determined in Section 4.2 is smaller than the value obtained by Davis &

Peebles (1983), though it is in excellent agreement with the value from the KOS survey. This may be a further indication that our sample is lacking in rich clusters. However, the relative peculiar velocities do not differ substantially from those deduced by Davis & Peebles (1983) which indicates that the estimates of $\langle w^2 \rangle$ are fairly stable. We have attempted to include the effects of sampling fluctuations, especially in the value of $Q$, in the error estimate given in equation (27).

(3) We have assumed that the galaxies are good tracers of the mass distribution. As discussed in Section 4.4, the weak dependence of $\langle w^2 \rangle^{1/2}$ with $\sigma$ provides evidence in support of this assumption, at least on scales $\lesssim r_0$. Further, Davis & Peebles (1983), using new redshift measurements, obtain $\langle w^2 \rangle^{1/2} \approx 200\,\mathrm{km\,s^{-1}}$ at $\sigma \approx 10\,h^{-1}\,\mathrm{kpc}$ from an analysis of the redshift distribution of Turner's sample of binaries (Turner 1976; White *et al.* 1983). This is not very different from the relative peculiar velocities between pairs with separations $\sim 1\,h^{-1}\,\mathrm{Mpc}$ showing that the slow variation of $\langle w^2 \rangle^{1/2}$ with $\sigma$ applies down to pair separations comparable to the optical radii of galaxies. However, it is difficult to rule out the possibility that a substantial fraction of the matter in the Universe is in a form which is weakly clustered on scales $\lesssim r_0$. If this were true, the cosmological density could be considerably greater than the estimate given in equation (27). A possible test of this hypothesis can be made by refining the estimate of $\Omega$ derived from an analysis of our infall velocity towards Virgo since this involves matter clumped on scales of about 15 Mpc. Current estimates lie within the range $0.1 < \Omega < 0.7$ (e.g. Aaronson *et al.* 1982; Davis & Huchra 1982; Hart & Davies 1982; Yahil 1981; Tonry & Davis 1980) which are not incompatible with the value presented here, though there is considerable scope for improvement.

In conclusion, our results suggest an open Universe with $\Omega = 0.14 \times 2^{\pm 1}$. The most important source of uncertainty in this estimate probably comes from point (3) above for it is not possible, using the present sample, to rule out the possibility that a weakly clustered dark component provides the dominant contribution to the mass density.

## Acknowledgments

We thank Marc Davis and Jim Peebles for sending us a copy of their preprint which motivated a more detailed discussion of streaming motions. AJB acknowledges the receipt of an SERC research studentship. GE thanks the SERC and King's College Cambridge for financial support. TS thanks the SERC for financial support.

## References

Aaronson, M., Huchra, J., Mould, J., Schechter, P. L. & Tully, R. B., 1982. *Astrophys. J.*, **258**, 64.
Clutton-Brock, M. & Peebles, P. J. E., 1981. *Astr. J.*, **86**, 1115.
Davis, M. & Huchra, J., 1982. *Astrophys. J.*, **254**, 437.
Davis, M. & Peebles, P. J. E., 1977. *Astrophys. J. Suppl. Ser.*, **34**, 425.
Davis, M. & Peebles, P. J. E., 1983. *Astrophys. J.*, **267**, 465.
Davis, M., Geller, M. J. & Huchra, J., 1978. *Astrophys. J.*, **221**, 1.
Efstathiou, G., 1983. In *Early Evolution of the Universe and its Present Structure, IAU Symp. No. 104,* eds Abell, G. O. & Chincarini, G., in press.
Efstathiou, G. & Eastwood, J. W., 1981. *Mon. Not. R. astr. Soc.*, **194**, 503.
Faber, S. M. & Gallagher, J. S., 1979. *A. Rev. astr. Astrophys.*, **17**, 135.
Fall, S. M., 1975. *Mon. Not. R. astr. Soc.*, **172**, 23P.
Fall, S. M., 1979. *Rev. Mod. Phys.*, **51**, 21.
Geller, M. J. & Peebles, P. J. E., 1973. *Astrophys. J.*, **184**, 329.
Groth, E. J. & Peebles, P. J. E., 1977. *Astrophys. J.*, **217**, 385.
Hart, L. & Davies, R. D., 1982. *Nature*, **297**, 191.
Huchra, J., Davis, M., Latham, D. & Tonry, J., 1983. *Astrophys. J. Suppl. Ser.*, **52**, 89.

Kirshner, R. P., Oemler, A. & Schechter, P. L., 1978. *Astr. J.,* **83,** 1549.
Kirshner, R. P., Oemler, A. & Schechter, P. L., 1979. *Astr. J.,* **84,** 951.
Peebles, P. J. E., 1974. *Astrophys. J.,* **189,** L51.
Peebles, P. J. E., 1976a. *Astrophys. J.,* **205,** L109.
Peebles, P. J. E., 1976b. *Astrophys. Space Sci.,* **45,** 3.
Peebles, P. J. E., 1979. *Astr. J.,* **84,** 730.
Peebles, P. J. E., 1980a. *The Large-Scale Structure of the Universe,* Princeton University Press, Princeton.
Peebles, P. J. E., 1980b. *Physical Cosmology,* p. 216, eds Balian, R., Audouze, J. & Schramm, D. N., North holland, Amsterdam.
Peebles, P. J. E., 1981. In *Proceedings of the Tenth Texas Symposium on Relativistic Astrophysics,* eds Ramaty, R. & Jones, F. C., *A. New York Acad. Sci.,* **375,** 157.
Peebles, P. J. E. & Groth, E. J., 1975. *Astrophys. J.,* **196,** 1.
Peebles, P. J. E. & Groth, E. J., 1976. *Astr. Astrophys.,* **53,** 131.
Rubin, V. C., Ford, W. K., Thonnard, N., Roberts, M. S. & Graham, J. A., 1976. *Astr. J.,* **81,** 687.
Schechter, P. L., 1976. *Astrophys. J.,* **203,** 294.
Schmidt, M., 1968. *Astrophys. J.,* **151,** 393.
Shanks, T., 1982. In *Progress in Cosmology,* ed. Wolfendale, A. W., Reidel, Dordrecht, Holland.
Shanks, T., Bean, A. J., Efstathiou, G., Ellis, R. S. & Peterson, B. A., 1983. *Astrophys. J.,* **274,** in press.
Shapley, H. & Ames, A., 1932. *Harvard Annals,* 88.
Soneira, R. M. & Peebles, P. J. E., 1977. *Astrophys. J.,* **211,** 1.
Soneira, R. M. & Peebles, P. J. E., 1978. *Astr. J.,* **83,** 845.
Tonry, J. & Davis, M., 1979. *Astr. J.,* **84,** 1511.
Tonry, J. & Davis, M., 1980. *Astrophys. J.,* **246,** 680.
Turner, E. L., 1976. *Astrophys. J.,* **208,** 20.
White, S. D. M., Huchra, J., Latham, D. & Davis, M., 1983. *Mon. Not. R. astr. Soc.,* **203,** 701.
Yahil, A., 1981. In *Proceedings of the Tenth Texas Symposium on Relativistic Astrophysics,* eds Ramaty, R. & Jones, F. C., *A. New York Acad. Sci.,* **375,** 169.